ICONHIC2022
3rd International Conference on Natural Hazards & Infrastructure
5-7 July 2022, Athens, Greece

A Risk-Based Design Procedure for Negative Stiffness Bilinear Elastic Systems

Natalia Reggiani Manzo[1], Michalis F. Vassiliou, Prof.
ETH Zurich

Christos G. Lachanas, Dimitrios Vamvatsikos, Prof.
National Technical University of Athens

ABSTRACT

This paper presents uniform risk spectra for systems with lateral negative stiffness, such as free-standing, restrained or curved-end rocking blocks. The spectra are constructed using a simplified system, the Zero Stiffness Bilinear Elastic system, which can satisfactorily predict the response of different systems with negative lateral stiffness. The paper offers the step-by-step methodology for the construction of the spectra. It presents the construction and discussion of the spectra for a site in Athens, Greece using two distinct intensity measures: Peak Ground Velocity and Peak Ground Acceleration.

Keywords: Uniform Risk Spectra, rocking spectra, nonlinear dynamics, negative stiffness

INTRODUCTION

Rocking has been extensively studied over the last half century (Agalianos et al., 2017; Aghagholizadeh & Makris, 2018; Dar et al., 2018; Dimitrakopoulos & Giouvanidis, 2015; Giouvanidis & Dimitrakopoulos, 2017; Housner, 1963; Makris & Vassiliou, 2013, 2014; Sieber et al., 2020; Thomaidis et al., 2020; Vassiliou et al., 2016, 2017; Vassiliou 2018; Zhang et al., 2019). However, it was only recently that the concept became increasingly popular and it was proposed as a seismic design method for resilient structures (Mashal & Palermo, 2019; Reggiani Manzo & Vassiliou, 2022; Rios-Garcia & Benavent-Climent, 2020; Sideris et al., 2014a, 2014b, 2015; Thonstad et al., 2016). A rocking column can reduce the forces transmitted to the foundation and, if designed with appropriate detailing (Mashal & Palermo, 2019; Reggiani Manzo & Vassiliou, 2021; Thonstad et al., 2016), present low-damage even after being subjected to its design earthquake.

The linearized lateral force-deformation relation of a free-standing rocking block presents negative stiffness and can be completely defined by two parameters: its uplifting force and maximum top horizontal displacement (Fig. 1a). The introduction of flexible non-prestressed restrainers increases the block's maximum horizontal displacement, while prestress also changes its uplifting force (Liu & Palermo, 2017; Makris & Vassiliou, 2015; Mashal & Palermo, 2019; Reggiani Manzo & Vassiliou, 2021; Sideris et al., 2014a, 2014b, 2015; Thomaidis et al., 2022; Thonstad et al., 2016; Vassiliou & Makris, 2015; Zhou et al., 2019). The block's uplifting force and maximum horizontal displacement can also be controlled by designing its ends in a curved shape (Fig. 1c) (Bachmann et al., 2017, 2019) or by adding damping or inerter devices (Aghaghoziladeh, 2020; Makris & Aghaghoziladeh, 2019; Thiers-Moggia & Málaga-Chuquitaype, 2019, 2020, 2021).

In seismic design, the current state of practice is to design structures using the uniform hazard spectrum (UHS), which define the seismic actions. Recently, Luco et al. (2007) proposed the Uniform Risk Spectra (URS), which does not provide seismic actions with uniform probability of exceedance (as the former), but it goes one

[1] reggianimanzo@ibk.baug.ethz.ch

step further and provides seismic actions that results in structures with uniform risk of damage and/or collapse. Both spectra represent key tools in practice that facilitate the seismic design of structures with positive stiffness. On the other hand, structures with negative stiffness cannot be designed using such spectra (Makris & Konstantinidis, 2003), and their design still depends on time history analyses.

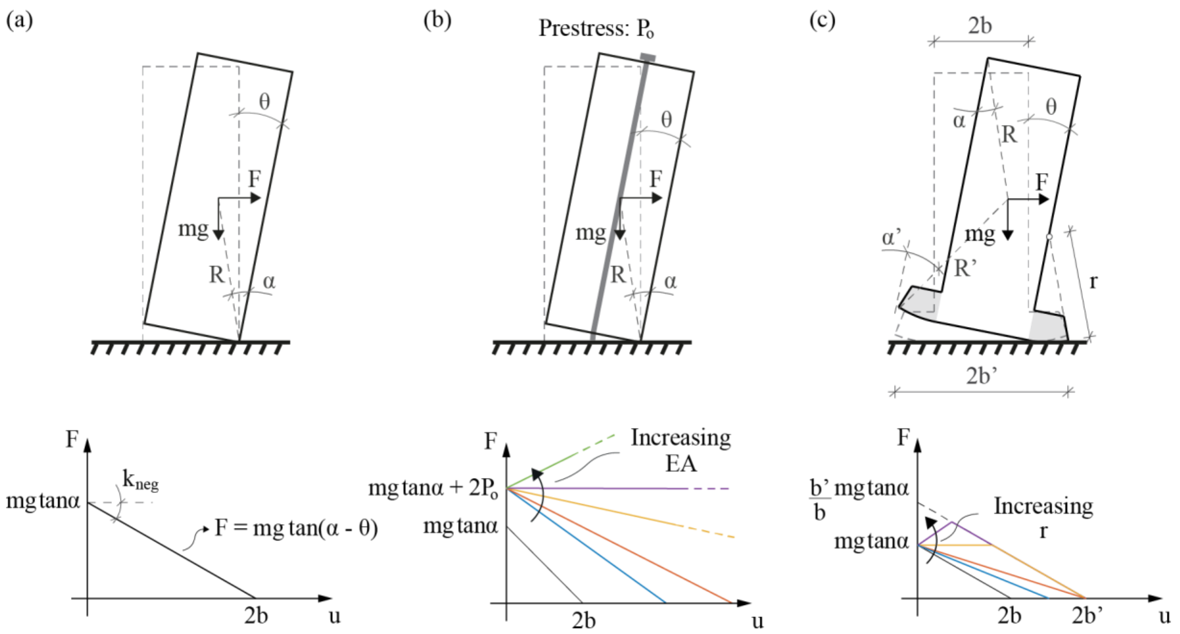

Figure 1. *(a) Free-standing rigid rocking block; (b) restrained rigid rocking block; and (c) curved-base rigid rocking block.*

Looking for simplified methods, Kazantzi et al. (2021) have offered normalized response prediction and fragility assessment expressions that can be employed within a probabilistic framework to assess or design simple rocking systems (Vamvatsikos & Aschheim, 2016). Following another approach, Reggiani Manzo & Vassiliou (2019, 2021) proposed a proxy system, the Zero Stiffness Bilinear Elastic (ZSBE) oscillator, which can be used to estimate the displacement demand of rocking systems with the same uplift force, but different maximum horizontal displacements. This simplified system reduces the number of variables in the rocking problem and allows the construction of a single spectrum for a range of negative stiffness systems: free-standing rocking frames, restrained rocking frames, or rocking frames with curved ends.

This paper further develops this simplified spectrum by considering the uncertainties inherent to seismic actions. It presents uniform risk spectra for a site in Athens, constructed using the ZSBE proxy, as well as the step-by-step methodology for its construction.

ZSBE AS A PROXY FOR NSBE

The Negative Stiffness Bilinear Elastic System

The Negative Stiffness Bilinear Elastic (NSBE) system can describe the dynamics of free-standing (Fig.1a), restrained (Fig.1b), and curved-based (Fig.1c) rocking structures, or any other deformable system that presents negative post-uplift stiffness and does not exhibit hysteretic damping. Fig. 2 presents the NSBE oscillator, and its displacement-restoring force relationship. Up until uplift, the system behaves as a linear single degree-of-freedom system, representing any deformability the system might present before uplifting. After uplifting, the tangent stiffness becomes negative (k_{neg}). The displacement capacity (u_{cap}) is defined not by material failure, but by the displacement that causes zero restoring force. Therefore, the displacement capacity of an unrestrained column measured at its top is equal to its width.

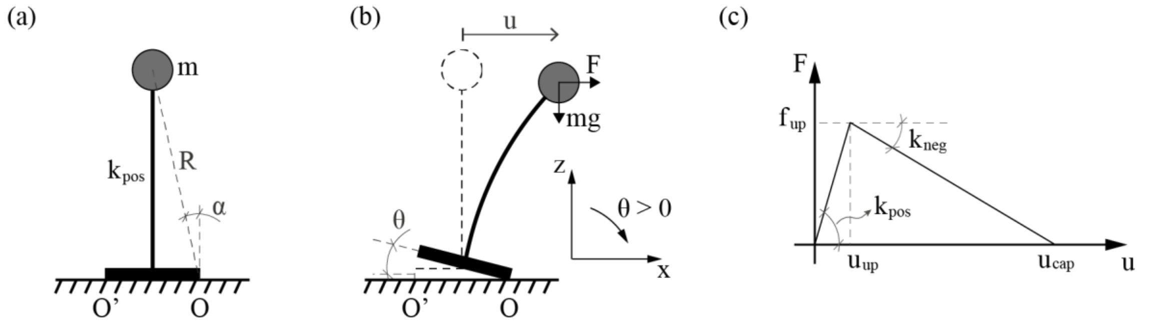

Figure 2. *(a, b) NSBE system representation; and (c) its displacement-restoring force relationship.*

Based on its displacement-force relationship (Fig. 2c), the oscillator's equation of motion is:

$$m \cdot \dot{u}(t) + f_{up} \cdot \frac{u(t)}{u_{up}} = -m \cdot \ddot{u}_g(t) \ , \quad |u(t)| \le u_{up} \tag{1}$$

$$m \cdot \ddot{u}(t) + \operatorname{sgn}\left(u(t)\right) \cdot f_{up} \cdot \left(\frac{u_{cap} - u(t)}{u_{cap} - u_{up}} \right) = -m \cdot \ddot{u}_g(t) \ , \quad |u(t)| > u_{up} \tag{2}$$

The only source of energy dissipation in the system is impact damping, which is assumed to happen instantaneously. This assumption is valid for rocking structures with protected ends and no extra damping mechanism but might deviate from reality when the column ends are not protected (Kalliontzis et al., 2016, 2020). When the system is returning to its original position and its displacement equals to the uplift displacement (u_{up}) (i.e. when the system is "downcrossing" u_{up}), the integration is halted, and its post-impact velocity is calculated by a coefficient of restitution (r_c):

$$r_c = \frac{\dot{u}_{post-impact}}{\dot{u}_{pre-impact}} \tag{3}$$

A coefficient of restitution equal to 0.95 is assumed, corresponding to relatively slender structures. It is known that the coefficient of restitution, as defined in Equation 3 and by Housner (1963), depends mainly on the slenderness of the column and consequently on the column's uplifting force. However, the uplifting force can also be changed without varying the coefficient of restitution by prestressing the rocking column (Makris & Vassiliou, 2015; Vassiliou & Makris, 2015).

The Zero Stiffness Bilinear Elastic System

Fig.3a presents the displacement-force relationship of the ZSBE system. The system follows the same equation of motion and assumptions of the NSBE system when its displacement capacity tends to infinity, resulting in a system with zero post-uplift stiffness (k_{neg} = 0).

The ZSBE oscillator can be used as a proxy for the prediction of the response of the NSBE oscillator (Reggiani Manzo & Vassiliou, 2019, 2021). Hence, studying the response of a ZSBE system of a given f_{up} and u_{up} suffices for the description of the response of all NSBE of the same f_{up} and u_{up}, independently of their u_{cap}. Therefore, spectra providing u_{max} of the ZSBE system as a function of f_{up} for a given u_{up} can be used for the design of NSBE systems. Fig.3b presents such a spectrum, extracted from Reggiani Manzo and Vassiliou (2021). It refers to u_{up} = 0.0005m and it gives the median response for a set of ground motions selected and scaled as discussed therein. Herein, a u_{up} = 0.0005m was also used to denote a quasi-rigid ZSBE system.

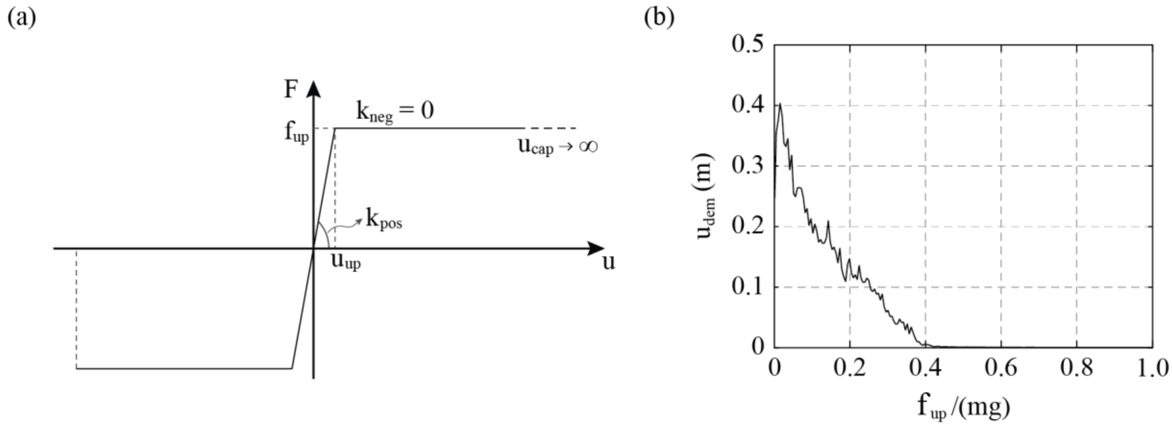

Figure 3. *(a) Displacement-restoring force relationship of the ZSBE system; and (b) spectrum obtained using the ZSBE proxy.*

METHODOLOGY FOR CONSTRUCTING THE UNIFORM RISK SPECTRA FOR NSBE SYSTEMS

Uniform hazard spectra (UHS) are widely adopted in seismic codes for the design of conventional structures. The UHS provides values of the (pseudo)spectral acceleration at different periods for a given mean annual frequency (MAF) of exceedance. Single-degree-of-freedom structures of a given period designed to reach "failure" (e.g. significant damage or life safety) at precisely the spectral acceleration value denoted by the UHS for this period would do so with the MAF (or equivalently the return period) that characterizes the UHS, assuming their response could be calculated without any uncertainty (Luco et al., 2007); typically, however, this is only the case for elastic oscillators and perfect knowledge. Any deviation from this strict norm results in increased MAFs, i.e., unconservative designs. Given the significant uncertainties inherent in nonlinear response, record-to-record variability, higher modes, geometry, and materials, this has become a well-known problem of intensity-based approaches. It is traditionally tackled by conventional design codes through ad hoc safety factors and overdesign, leading to the advent of performance-based seismic design (PSBD, (Vamvatsikos & Aschheim, 2016; Krawinkler et al., 2006)).

Given the computational complexity of early PSBD approaches, Luco et al. (2007) tried to strike a middle ground by proposing the Risk-Targeted or Uniform Risk Spectrum (URS). The URS provides seismic actions that at least results in elastoplastic single-degree-of-freedom systems with uniform risk of damage or collapse, partially mitigating some of the inaccuracies of the UHS when applied to realistic systems (Spillatura, 2018). Therefore, given the practicality of the URS for seismic design, this paper demonstrates how to produce them for ZSBE systems.

Using the ZSBE proxy, the proposed URS is a plot of the displacement demand of the system as a function of its normalized strength, in which all ordinates of the plot present the same MAF of exceedance (Fig. 4b). The URS can also be interpreted as an iso-MAF contour plot of the seismic risk surface, which is a three-dimensional plot of the annual probability of exceeding a displacement demand for a range of systems with different normalized uplifting forces (Fig. 4a).

The calculation of the probability of exceedance is performed using the risk integral (Cornell et al., 2002):

$$\lambda_{LS} = \lambda\left(EDP > EDP_C\right) = \int P\left(EDP > EDP_C \mid IM\right) \cdot \left|d\lambda\left(IM\right)\right| \tag{4}$$

in which λ_{LS} is the mean annual frequency (MAF) of exceeding (i.e., violating) a limit state (LS), $P(EDP > EDP_C \mid IM)$ is the fragility function, which represents the probability that the engineering demand parameter (*EDP*) exceeds the capacity threshold of EDP_C associated with *LS* for any given level of the ground motion intensity measure (*IM*) and $\lambda(IM)$ is the MAF of exceeding a given value of *IM*, which can be retrieved from the site-specific seismic hazard curve. Note that Equation 4 gives a single-point of the seismic risk surface. To construct the complete surface, the equation has to be evaluated for several limit states and a range of systems with different normalized uplifting force (i.e. $f_{up}/(mg)$).

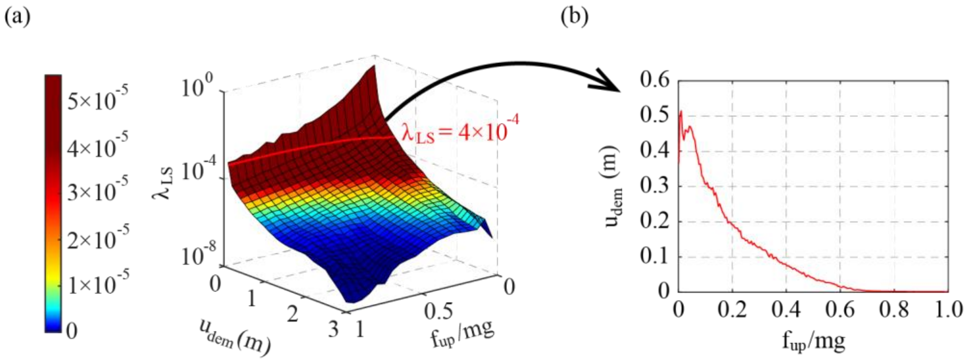

Figure 4. *(a) Seismic risk surface with an iso-MAF contour plot highlighted; and (b) Uniform Risk Spectrum.*

Intensity measures (IMs)

Given that all outputs of the risk assessment are conditioned on the chosen IM, it is extremely important to choose it wisely (Kazantzi & Vamvatsikos, 2015). However, no consensus exists in the engineering community of which IM is the most adequate for rocking structures. To guarantee hazard computability, two commonly used IMs in vulnerability studies are employed herein, namely the *PGA* and *PGV*. Both are employed in their geomean form, denoted henceforth as $\overline{PGA}$ and $\overline{PGV}$, and calculated as the geometric mean of the *PGA* and *PGV*, respectively, from the two horizontal components (x, y) of the ground motions:

$$\overline{PGV} = \sqrt{PGV_x \cdot PGV_y} \tag{5}$$

$$\overline{PGA} = \sqrt{PGA_x \cdot PGA_y} \tag{6}$$

Site-specific seismic hazard curve

The risk assessment was conducted for a site in Athens, Greece (Vamvatsikos et al., 2020). The seismic hazard curves for both IMs were assessed via Probabilistic Seismic Hazard Analysis (PSHA (Cornell, 1968)). For the hazard calculations, the open-source platform OpenQuake (2016) was used with the 2013 European seismic hazard model (ESHM13, (Woessner et al., 2015)). From the available logic tree branches of ESHM13 only the area source model and the Boore Atkinson 2008 GMPE (Boore & Atkinson, 2008) were employed. Since no site-specific data for the soil condition were available, a uniform "rock" soil type was assumed (V_{S30} = 800 m/s) in the present study.

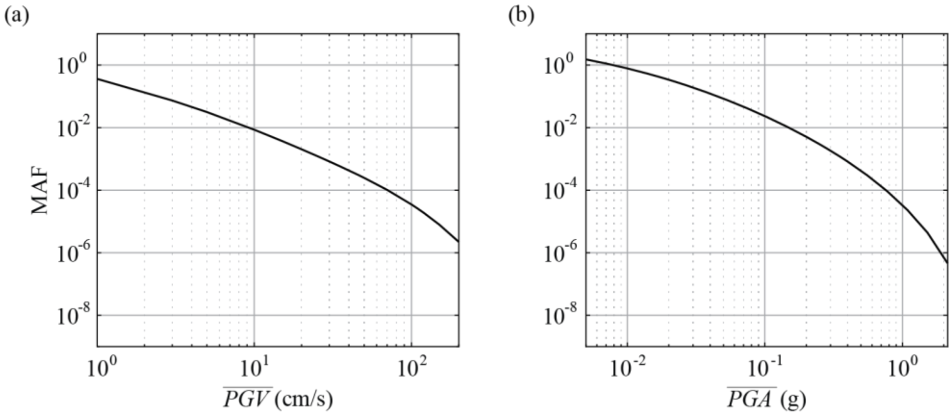

Figure 5. *Seismic mean hazard curve for a site in Athens, Greece, using (a)* $\overline{PGV}$ *and (b)* $\overline{PGA}$ *as IM.*

Fragility curves

Incremental dynamic analyses (IDA) (Vamvatsikos & Cornell, 2002) were carried out to obtain the fragility functions for each predefined limit state and system. A set of 105 firm-soil ordinary (no-pulse, no-long-duration) ground motions were selected from the PEER database (PEER NGA Database, 2005; Chiou et al., 2008). When adopting $\overline{PGV}$ as IM, the ground motions were gradually scaled in $\overline{PGV}$ levels of: $\overline{PGV} = \left[(1:0.5:20),(25:5:200)\right]$ cm/s. For the $\overline{PGA}$, scaling was employed in specific levels of: $\overline{PGA} = \left[0.001,(0.0025:0.0025:0.0225),(0.025:0.005:0.195),(0.20:0.05:2)\right]$ g.

The ZSBE system's model considers only planar response. Therefore, the nonlinear dynamic analysis was carried out only for one of the components of each ground motion (arbitrary component). The component was chosen once randomly, and then used for all analyses. After carrying out the analyses for all different scales and ground motions, the fragility function per limit state and system can be easily obtained on an *EDP* or and IM-basis approach (Bakalis & Vamvatsikos 2018). In this paper, the former was employed. For each IM-step value (stripe), the probability of exceeding the deterministic *EDP* capacity threshold was calculated as:

$$P\left(EDP > EDP_C \mid IM\right) = \frac{\text{number of records with } EDP > EDP_C}{\text{total number of records}} \tag{7}$$

Note that for smaller values of $\overline{PGV}$ and $\overline{PGA}$, a finer discretization was adopted because low *PGV* or *PGA* ground motions might lead to smaller *EDP* values, but they also have large probability of occurrence, hence resulting in significant contribution to the convolution of the risk integral (Equation 4).

The maximum horizontal displacement of the system (u_{dem}) was adopted as the *EDP*. To construct the seismic risk surface (Fig. 4a), fragility curves were constructed for several limit states and a range of systems with different normalized uplifting force. Herein, 3002 thresholds were evaluated, ranging from 0 to 3 m, in steps of 0.001 m. To be able to depict uplift, the threshold 0.0005 m was also included. The nonlinear analyses were carried out for systems with normalized uplifting force varying from 0.1 to 1.0, in steps of 0.05.

Risk Integral

The last step for obtaining the probability of exceedance (λ_{LS}, Equation 4) was to combine the structural response (i.e. fragility curves) with the seismic hazard at each location. The evaluation of the risk integral for all 3002 thresholds and 301 systems with distinct normalized uplifting force, resulted in the seismic risk surface. Herein, the URS with 2%, 10% and 50% probability of exceedance in 50 years are presented. These probabilities correspond to a MAF of 0.0004, 0.0021 and 0.0139 per year, as given by Equation 8, in which MAF can be converted to probability of exceedance (P_T) in a specific period of time (T), and vice versa, via the cumulative distribution function of the exponential distribution:

$$\mathrm{MAF} = \frac{-\ln(1-p)}{T} \tag{8}$$

UNIFORM RISK SPECTRA

Fig. 6 presents the URS with 2%, 10% and 50% probability of exceedance in 50 years, constructed using $\overline{PGV}$ and $\overline{PGA}$ as IM, respectively. As expected, for both IMs, the displacement demands are increased when moving from the less frequent hazard levels (i.e., 2% in 50 years) to the most frequent.

Observing the spectra constructed for the same probability of exceedance, but different IMs, one can infer that the $\overline{PGA}$-based spectra predict larger displacement demands than the spectra that adopt $\overline{PGV}$ as *IM*. The larger displacement demands could be a consequence of the higher variance that Ground Motion Prediction Equations (GMPE) for $\overline{PGA}$ present in comparison to GMPEs for $\overline{PGV}$. From Equation 4 it follows that distributions with fatter tails, once convolved with the fragility curves, lead to larger risk values.

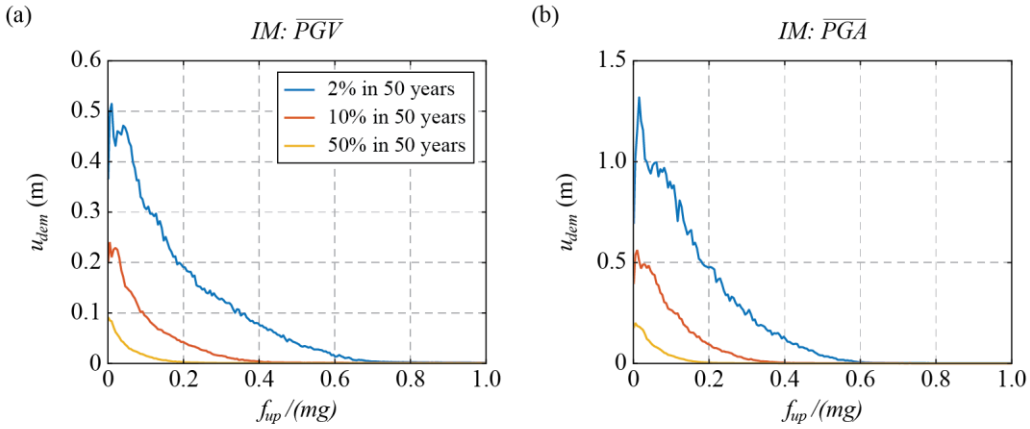

Figure 6. *Uniform risk spectra for rocking structures with 2%, 10% and 50% probability of exceedance in 50 years, constructed using (a)* $\overline{PGV}$ *and (b)* $\overline{PGA}$ *as IM.*

CONCLUSIONS

Using the Zero Stiffness Bilinear Elastic (ZSBE) system as a proxy for rocking systems, this paper constructed uniform risk displacement demand spectra for rocking structures, which could be used for their preliminary design. After explaining the methodology for constructing the spectra, the paper presented spectra for a site in Athens, Greece, which were constructed using two distinct intensity measures ($\overline{PGA}$ and $\overline{PGV}$).

ACKNOWLEDGEMENTS

This work was supported by the ETH Zurich under grant ETH-10 18-1. The authors would also like to acknowledge the financial support provided by the European Framework Programme for Research and Innovation (Horizon 2020) under the “YADES” Marie Skłodowska-Curie project with Grant Agreement No 872931.

REFERENCES

Agalianos A., Psychari A., Vassiliou MF., Stojadinovic B., Anastasopoulos I. (2017). Comparative assessment of two rocking isolation techniques for a motorway overpass bridge. *Front. Built Environ.*, *3*, 1–19.

Aghagholizadeh M. & Makris N. (2018). Earthquake response analysis of yielding structures coupled with vertically restrained rocking walls. *Earthq. Eng. Struct. Dyn., 47*(15), 2965–2984.

Aghagholizadeh, M. (2020). A finite element model for seismic response analysis of vertically-damped rocking-columns. *Engineering Structures, 219*, 110894.

Bachmann JA., Vassiliou MF., Stojadinovic B. (2017). Dynamics of rocking podium structures. *Earthq. Eng. Struct. Dyn., 46*(14), 2499–2517.

Bachmann JA., Vassiliou MF., Stojadinovic B. (2019). Rolling and rocking of rigid uplifting structures. *Earthq. Eng. Struct. Dyn., 48*(14), 1556–1574.

Baker JW., Cornell CA. (2006). Which spectral acceleration are you using?. *Earthquake Spectra, 22*(2), 293-312.

Bakalis K, Vamvatsikos D. (2018). Seismic fragility functions via nonlinear response history analysis. *Journal of Structural Engineering (ASCE), 144*(10), 04018181.

Boore DM., Atkinson GM. (2008). Ground-motion prediction equations for the average horizontal component of PGA, PGV, and 5% damped PSA at spectral periods between 0.01s and 10.0s. *Earthquake Spectra, 24*(1), 99–138.

Chiou B., Darragh R., Gregor N., Silva W. (2008). NGA Project Strong-Motion Database. *Earthquake Spectra, 24*(1), 23–44.

Cornell CA. (1968). Engineering seismic risk analysis. *Bulletin of the Seismological Society of America, 58*(5), 1583-1606.

Cornell CA., Jalayer F., Hamburger RO., Foutch DA. (2002). Probabilistic basis for 2000 SAC federal emergency management agency steel moment frame guidelines. *Journal of Structural Engineering, 128*(4), 526-533.

Dar A., Konstantinidis D., El-Dakhakhni W. (2018). Seismic response of rocking frames with top support eccentricity. *Earthq. Eng. Struct. Dyn., 47*(12), 2496–2518.

Dimitrakopoulos EG. & Giouvanidis AI. (2015). Seismic Response Analysis of the Planar Rocking Frame. *J. Eng. Mech., 141*(7), 04015003.

Giouvanidis AI. & Dimitrakopoulos EG. (2017). Seismic Performance of Rocking Frames with Flag-Shaped Hysteretic Behavior. *J. Eng. Mech., 143*(5), 04017008.

Housner GW. (1963). The behaviour of inverted pendulum structures during earthquakes. *Bull. Seismol. Soc. Am., 53*(2), 403-417, 1963.

Kalliontzis D., Sritharan S., Schultz A. (2016). Improved Coefficient of Restitution Estimation for Free Rocking Members. *J. Struct. Eng., 142*(12), 06016002.

Kalliontzis, D., & Sritharan, S. (2020). Dynamic response and impact energy loss in controlled rocking members. *Earthquake Engineering & Structural Dynamics, 49*(4), 319-338.

Kazantzi AK. & Vamvatsikos D. (2015). Intensity measure selection for vulnerability studies of building classes. *Earthq. Eng. Struct. Dyn., 44*(15), 2677-2694.

Kazantzi AK., Lachanas CG., Vamvatsikos D. (2021). Seismic response distribution expressions for on-ground rigid rocking blocks under ordinary ground motions. *Earthq. Eng. Struct. Dyn. 50*(12), 3311-3331.

Krawinkler H., Zareian F., Medina RA., Ibarra LF. (2006). Decision support for conceptual performance-based design. Earthq. Eng. Struct. Dyn., 35(1), 115-133.

Liu R, Palermo A. (2017). Quasi-Static Testing of a 1/3 Scale Precast Concrete Bridge Utilising a Post-Tensioned Dissipative Controlled Rocking Pier. In *Proceedings of 16th World Conference on Earthquake Engineering*.

Luco N., Ellingwood BR., Hamburger RO., Hooper JD., Kimball JK., Kircher CA. (2007). Risk-targeted versus current seismic design maps for the conterminous United States. *Struct. Eng. Assoc. Calif. 2007 Conv. Proc.*, 1–13.

Makris N., Aghagholizadeh M. (2019). Effect of supplemental hysteretic and viscous damping on rocking response of free-standing columns. *Journal of Engineering Mechanics, 145*(5), 04019028.

Makris N. & Konstantinidis D. (2003). The rocking spectrum and the limitations of practical design methodologies. *Earthq Eng Struct Dyn., 32*(2), 265-289.

Makris N. & Vassiliou M. (2013). Planar rocking response and stability analysis of an array of free-standing columns capped with a freely supported rigid beam. *Earthq. Eng. Struct. Dyn., 42*(3), pp. 431–449.

Makris N. & Vassiliou MF. (2014). Are Some Top-Heavy Structures More Stable?. *J. Struct. Eng., 140*(5), 06014001.

Makris N. & Vassiliou MF. (2015). Dynamics of the Rocking Frame with Vertical Restrainers. *J. Struct. Eng., 141*(10), 04014245.

Mashal M. & Palermo A. (2019). Low-damage seismic design for accelerated bridge connection. *J. Bridge Eng., 24*(7), 04019066.

Global Earthquake Model [GEM]. (2016). OpenQuake Engine User Instruction Manual.

PEER NGA Database. *Pacific Earthquake Engineering Research Center*, Berkeley, CA, 2005. http://peer.berkeley.edu/nga/ (Acessed on Jul. 27, 2021).

Reggiani Manzo N. & Vassiliou MF. (2019). Displacement-based analysis and design of rocking structures. *Earthq. Eng. Struct. Dvyn., 48*(14), 1613-1629.

Reggiani Manzo N. & Vassiliou MF. (2021). Simplified analysis of bilinear elastic systems exhibiting negative stiffness behavior. *Earthq. Eng. Struct. Dyn., 50*(2), 580–600.

Reggiani Manzo N. & Vassiliou M. (2021). Cyclic tests of a precast restrained rocking system for sustainable and resilient seismic design of bridges. *Eng. Struct.*

Ríos-García G. & Benavent-Climent A. (2020). New rocking column with control of negative stiffness displacement range and its application to RC frames. *Eng. Struct., 206*, 110133.

Sideris P., Aref AJ., Filiatrault A. (2014a). Quasi-Static Cyclic Testing of a Large-Scale Hybrid Sliding-Rocking Segmental Column with Slip-Dominant Joints. *J. Bridg. Eng., 19*(10), 04014036.

Sideris P., Aref AJ., Filiatrault A. (2014b). Large-Scale Seismic Testing of a Hybrid Sliding-Rocking Posttensioned Segmental Bridge System. *J. Struct. Eng., 140*(6), 04014025.

Sideris P., Aref AJ., Filiatrault A. (2015). Experimental Seismic Performance of a Hybrid Sliding–Rocking Bridge for Various Specimen Configurations and Seismic Loading Conditions. *J. Bridg. Eng., 20*(11), 04015009.

Sieber M., Klar S., Vassiliou MF., Anastasopoulos I. (2020). Robustness of simplified analysis methods for rocking structures on compliant soil. *Earthq. Eng. Struct. Dyn., 49*(14), 1388–1405.

Spillatura, A. (2018). *From record selection to risk targeted spectra for risk-based assessment and design* (Doctoral dissertation, Istituto Universitario degli Studi Superiori (IUSS)).

Thiers-Moggia R., Málaga-Chuquitaype C. (2019). Seismic protection of rocking structures with inerters. *Earthq. Eng. Struct. Dyn., 48*(5), 528–547.

Thiers-Moggia R., Málaga-Chuquitaype, C. (2020). Seismic control of flexible rocking structures using inerters. *Earthquake Engineering & Structural Dynamics, 49*(14), 1519-1538.

Thiers-Moggia R., Málaga-Chuquitaype, C. (2021). Effect of Base-Level Inerters on the Higher Mode Response of Uplifting Structures. *Journal of Engineering Mechanics*, *147*(8), 04021041.

Thomaidis IM., Kappos AJ., Camara A. (2020). Dynamics and seismic performance of rocking bridges accounting for the abutment-backfill contribution. *Earthq. Eng. Struct. Dyn., 49*(12), 1161–1179.

Thomaidis IM., Camara A., Kappos AJ. (2022). Dynamics and seismic performance of asymmetric rocking bridges. *Journal of Engineering Mechanics, 148*(3), 04022003.

Thonstad T., Mantawy IM., Stanton JF., Eberhard MO., Sanders DH. (2016). Shaking table performance of a new bridge system with pretensioned rocking columns. *J. Bridge Eng., 21*, 04015079.

Vamvatsikos D., Cornell CA. (2002). Incremental dynamic analysis. *Earthq. Eng. Struct. Dyn., 31*(3), 491-514.

Vamvatsikos D., Aschheim MA. (2016). Performance-based seismic design via Yield Frequency Spectra. *Earthq. Eng. Struct. Dyn., 45*(11), 1759-1778.

Vamvatsikos D., Bakalis K., Kohrangi M., Pyrza S., Castiglioni C., Kanyilmaz A., Morelli F., Stratan A., D'Aniello M., Calado L., Proença JM., Degee H., Hoffmeister B., Pinkawa M., Thanopoulos P., Vayas I. (2020). A risk-consistent approach to determine EN1998 behaviour factors for lateral load resisting systems. *Soil Dynamics and Earthquake Engineering, 131*, 106008.

Vassiliou MF. & Makris N. (2015). Dynamics of the Vertically Restrained Rocking Column. *J. Eng. Mech., 141*(12), 04015049.

Vassiliou MF., Mackie KR., Stojadinovic B. (2016). A finite element model for seismic response analysis of deformable rocking frames. *Earthq. Eng. Struct. Dyn., 46*(3), 447–466.

Vassiliou MF., Burger S., Egger M., Bachmann JA., Broccardo M., Stojadinovic B. (2017). The three-dimensional behavior of inverted pendulum cylindrical structures during earthquakes. *Earthq. Eng. Struct. Dyn., 46*(14), 2261–2280.

Vassiliou MF. (2018). Seismic response of a wobbling 3D frame. *Earthq. Eng. Struct. Dyn., 47*(5), 1212–1228.

Woessner J., Larentiu D., Giardini D. *et al.* (2015). The 2013 European Seismic Hazard Model: key components and results. *Bull. Earthq. Eng., 13*, 3553-3596.

Zhang J., Xie Y., Wu G. (2019). Seismic responses of bridges with rocking column-foundation: A dimensionless regression analysis. *Earthq. Eng. & Struct. Dyn.*, *48*(1), 152-170.

Zhou YL., Han Q., Du XL., Zhang JQ., Cheng SS., Chen JY. (2021). Additional viscous dampers for double-column rocking bridge system: Seismic response and overturning analysis. *Soil Dyn. Earthq. Eng., 141*, 106504.

Zhou YL., Han Q., Du XL., Jia Z. (2019). Shaking Table Tests of Post-Tensioned Rocking Bridge with Double-Column Bents. *J. Bridg. Eng.*, *24*(8), 04019080.